



Characteristics investigation on heat transfer growth of sonochemically synthesized ZnO-DW based nanofluids inside square heat exchanger

Waqar Ahmed^{1,2} · Z. Z. Chowdhury³ · S. N. Kazi² · MR. Johan³ · Naveed Akram^{2,4} · C. S. Oon^{2,5} · Ali H. Abdelrazek²

Received: 16 November 2019 / Accepted: 17 March 2020 / Published online: 4 April 2020
© Akadémiai Kiadó, Budapest, Hungary 2020

Abstract

In recent decades, the growth of heat transfer using nanomaterials in the conventional base fluid has caught the attention of researchers around the world. The present research investigates the growth in heat transfer using ZnO-DW based nanofluids in a square heat exchanger. ZnO nanoparticles were synthesized by using the single-pot sonochemical technique. The ZnO-DW based nanofluids with different concentrations (0.1, 0.075, 0.05 and 0.025 mass%) were prepared by using probe sonication technique. The heat transfer growth will be benchmarked using the experimental data from distilled water experiment. Reynolds numbers, average convective heat transfer coefficient (h), and Nusselt number were calculated and analyzed in this investigation. Significant enhancement of 52% in thermal conductivity was noticed at 45 °C for 0.1 mass% concentration of ZnO-DW based nanofluids, which is due to the presence of maximum ZnO nanoparticles. Moreover, the maximum improvement in Nusselt values recorded at the end of the square pipe is 47% for 0.1 mass%, while 32%, 27% and 17% increase was recorded for 0.075, 0.05 and 0.025 mass% concentrations, and heat transfer enhancement was from 500 to 1100, 500 to 960, 500 to 910, and 500 to 900 W m⁻² K⁻¹ for different ZnO-DW based nanofluids mass% concentrations, which is more than water due to stability of nanoparticles. It can be concluded that the heat transfer performance enhancement is credited to the combination of square pipe and well-dispersed and stable ZnO-DW based nanofluids for heat exchanger applications.

✉ Waqar Ahmed
waqarum.ah@gmail.com

✉ S. N. Kazi
salimnewaz@um.edu.my

¹ Institute of Advanced Studies, University of Malaya,
50603 Kuala Lumpur, Malaysia

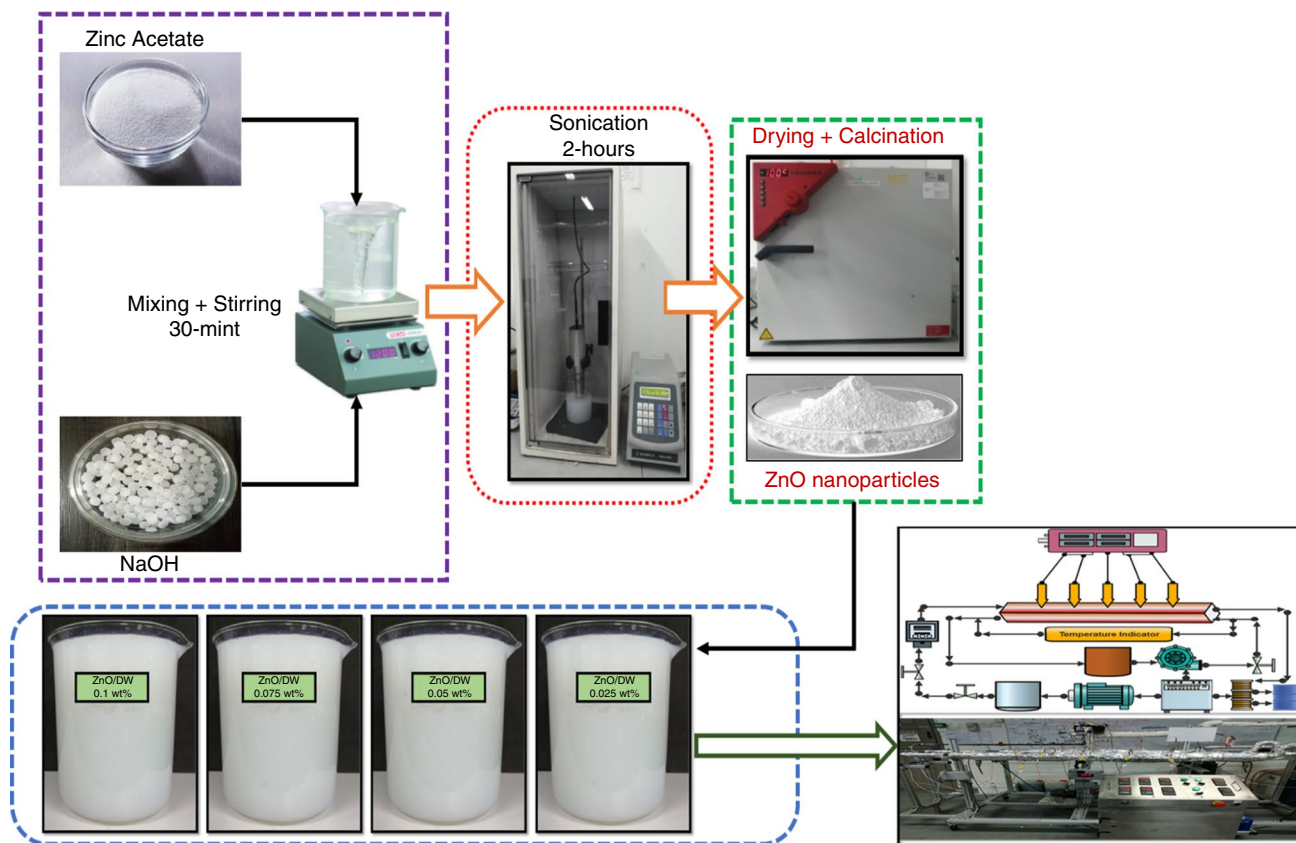
² Department of Mechanical Engineering, Faculty
of Engineering, University of Malaya, 50603 Kuala Lumpur,
Malaysia

³ Nanotechnology and Catalysis Research Center, NANOCAT,
Kuala Lumpur, Malaysia

⁴ Departmenet of Mechanical Engineering, Mirpur University
of Science and Technology(MUST), Mirpur, AJK 10250,
Pakistan

⁵ School of Engineering, Monash University,
47500 Bandar Sunway, Malaysia

Graphic abstract



Keywords Synthesis of ZnO · ZnO-DW based nanofluid · Convective heat transfer · Thermal conductivity · Reynolds and Nusselt numbers

List of symbols

A	The inner area of pipe
D_h	Hydraulic diameter
C_p	Heat capacity for nanofluid
P_p	System pumping power
Q	Heat flux
mass%	Nanoparticles mass concentration
k	Thermal conductivity ($\text{W m}^{-1} \text{K}^{-1}$)
I	Inlet condition
PN	Prantadel numbers ($\text{Pr} = c_p \cdot \eta / k$)
S_{gen}	Entropy ratio
B	Bulk value
c_p	Specific heat ($\text{J kg}^{-1} \text{K}^{-1}$)
Re	Reynolds numbers ($\text{Re} = \rho \cdot v \cdot D / \eta$)
T_{out}	Outlet temperature of fluid
T_{in}	Inlet temperature of fluid
T_s	Pipe surface temperature
T_b	Fluid bulk temperature
V	Velocity (m s^{-1})

Subscript

nf	Nanofluid
bf	Value of base fluid
np	Nanoparticle
r	Ratio

Greek symbols

μ	Dynamical viscosity (MPa s)
ρ	Fluid density in (kg m^{-3})
ω	Mass concentration (%)

Abbreviations

ff	Friction factor
PEG	Poly ethylene glycol
TEM	Transmission electron microscopy
DW	Distilled water
TC	Thermocouple
HVAC	High-voltage alternating current

Introduction

The research on convective heat transfer enhancement in engineering industries has ever been essential due to the rapidly growing demand for energy savings. Heat exchangers have been used for transportation, chemical processing, food industry, and many other engineering applications. Generally, heat exchangers use conventional heat transfer liquids like water, ethylene glycol, a mixture of them, etc., as the working fluid; however, due to low thermal conductivity, their heat transfer coefficients were low and could not transport heat at a higher rate. Later, it was realized that the dispersion of solid metal nanoparticles in base fluid enhanced the thermal conductivity of the fluid as compared to the conventional base fluid [1, 2]. Massive-scale researches on dispersion and stability of solid nanoparticles (metal oxides and carbon-based) in the base fluid for enhancement of heat transfer values have been carried out [2]. However, it noticed due to greater particle size, settling, sedimentation, clogging, and erosion occurred, which decrease heat transfer and thermal conductivity. To solve these issues, many researchers prepared different nanofluids for investigation on the enhancement of thermal conductivity and heat transfer [3, 4]. nanofluids, using metal oxides like (Al_2O_3 , TiO_2 , Fe_3O_4 , CuO , MgO) and SiO_2 , were also investigated by different researchers for enhanced thermal conductivity [5–7].

Different nanomaterials retain higher mechanical, electrical, optical and thermal properties, due to which they became appropriate for different applications. Some past studies expose many advancements in measuring and modeling of different thermophysical properties nanoparticles and their respective nanofluids. For the subject purpose, different thermophysical properties, like thermal conductivity, viscosity, thermal diffusivity, density, specific heat etc., and their optimistic effects on heat transfer improvement of different heat exchangers have been introduced. The key factors which affect these properties are nanoparticle size, morphology of particles, concentration of particles, aggregation, and maximum sonication time that is deliberate. Furthermore, these properties not only bound to the single fluids, but also applicable for composite/hybrid nanofluids for heat transfer improvements [8, 9]. Wen and Ding et al. [14] conducted the experiment using the nanoparticles to enhance the thermal conductivity of the fluids. Many other researchers also reported, with the mixing of highly conductive solid nanoparticles in the base fluid cause to enhance the thermal conductivity which plays important role to improve the heat transfer in different heat exchangers [10]. Some researchers reported the occurrence of the nanoparticles in a fluid will increase the chaotic movement of the nanofluid so that it becomes

more turbulence and the heat transfer will be increased and also concluded that the size and shape of the nanoparticles also caused the enhancement of heat transfer of the nanofluids. The different analysis suggested that the higher volume of concentration of the nanofluid will produce higher heat transfer rate, and the smaller size of nanoparticles increases the viscosity of nanofluid, which leads to improvement in heat transfer and Nusselt values [11, 12].

Several kinds of researches on dispersion and stability of solid nanoparticles in base fluid for enhancement of heat transfer values have been carried out in recent decades. However, many problems were identified when particles were mixed in the working fluids. The problem can be due to particle size, settling, sedimentation, clogging and erosion which will affect the heat transfer and overall performance of heat exchanger. In order to eradicate the problems, many researchers tested different nanofluids, geometry, and configurations of the heat exchanger to enhance the heat transfer [13]. Some other researchers also studied nanofluids using different metal oxides like (Al_2O_3 , TiO_2 , Fe_3O_4 , CuO) and SiO_2 also as a working fluid for heat exchanger; it was found that thermal conductivity enhancement contributes to overall heat transfer of the various heat exchanger tube geometry [7, 14, 15].

Porous substances saturated with Water and ZnO based nanofluids are being used for heat transfer improvement in a tilted hemispherical inclusion which vault is preserved isothermally while their disc is a more active electronic assembly is generating greater heat flux. An experimental setup has been intended to calculate the average Nusselt values for different mixtures gained by changing different physical constraints such as nanofluid disk generated power, volume fraction, thermal conductivities of porous passage and disk's inclination related to the field gravity [16]. Nanofluids were primed by using the two-step method at 0.1 mass%, and 0.3 mass%, respectively. Outcomes exposed that the occurrence of ($\text{MgO}/\text{therminol 66}$) rises the flow boiling convective heat transfer coefficient as compared with base fluids. Conversely, with a rise in the wt. concentrations of nanoparticle, the convective heat transfer decreases. Results also exposed that bubble creation persuades a pressure drop inside the subjected test section. Heat flux needed no effect on the overall pressure drop, where the rise in the nanofluid flow rates triggered a rise in the overall pressure drop [17].

The composites/hybrid nanofluids are innovative nanofluids primed by suspending a different kind of nanoparticles also in blend or composite form. These nanofluids are capable to enhance the heat transfer rate in different heat exchangers depending upon their design and structure. Also, addition of different nanoparticles together in base fluid can change their thermophysical properties and can effect to heat transfer [18–20]. Actually, for the fabrication of composites/

hybrid nanofluids, more than two different nanoparticles are used, and one of the composites/hybrid nanofluids comprises CNTs (carbon nanotubes) and the other is magnetic nanoparticle. Functionalizing CNTs (carbon nanotubes) applying magnetic nanoparticles can syndicate the properties of CNTs and different magnetic nanoparticles, which can formulate nanomaterials with changes in physical and chemical properties. In fact, the magnetic nanoparticle attaches to CNT's wall through hydrophobic connections [21–23]. An effort has been conducted to examine dispersion, stability and thermophysical characteristics of Cu-engine oil-based nanofluids and to find the major factors for choosing a consistent model to calculate their thermal conductivities and viscosity value in the absence of physical experimental set up [20, 24]. Functional nanofluids in subject study specified moral dispersion and stability in determining zeta potential values by means of the statistic that preparation methods of nanofluids in this research were considered as one-step technique and this type is directed to virtuous stability compared to two-step method [25, 26].

Conventional heat exchange liquids, such as water, oil, and EG, are generally utilized in different mechanical fields including auto motives, HVAC, car assembling unit, air transportation, astronautics, etc. All these customary heat exchange liquids are nonetheless often restricted by their unsatisfactory properties specifically lower heat conductivity and higher thickness, which infers that colossal heat

exchangers and incredible siphons would be connected to the power cycle framework [27, 28]. A notable number of investigations have been performed utilizing Al_2O_3 , TiO_2 , CuO , or metallic nanoparticles dispersed in water, EG, and PEG nanofluids. Limited works on ZnO /water nanofluid have been reported and no notable work was done on a blend of ZnO /water nanofluids for heat exchange and transport properties. From the previous literature, Table 1 describes the rheological parameters for different metal oxide-based nanofluids. Density, heat transfer, thermal conductivity [29, 30] are compared in the current research.

In addition, the rapid development in nanotechnology helped to prepare efficient nanofluids that replaced the traditional inefficient heat transfer fluids [31, 32]. In industries, nanoparticles dispersed in nanofluids have distinct importance due to their stable suspensions in the liquids and higher thermal performance. It has been observed that nanofluids could play a positive role in thermal conductivity and heat transfer enhancements [33]. Moreover, single-phase nanofluids synthesized from EG/water or PEG/water were used for convective heat transfer investigation and significant heat transfer performance was noted in some cases. According to the literature, the heat convection of nanofluids is one of the desired fields of research like many thermodynamic properties [34]. Many investigations on convection utilizations of TiO_2 , Al_2O_3 , CuO nanofluids have reported, but moderately little consideration has

Table 1 Measured rheological properties of water and different metal oxide-based nanofluids

S. no	Fluid type	vol%	Density/kg m ⁻³	Convective heat capacity/J kg ⁻¹ K ⁻¹	Thermal conductivity/W mK ⁻¹	Viscosity/mPa
1	Water	0	992	4182	0.618	0.62
2	Al_2O_3	0.5	1002	4110	0.642	0.67
3	Al_2O_3	0.75	1007	4099	0.652	0.69
4	Al_2O_3	1.0	1013	4091	0.659	0.70
5	Al_2O_3	1.25	1016	4062	0.667	0.71
6	Al_2O_3	1.5	1019	4035	0.674	0.73
7	Al_2O_3	2.0	1026	3983	0.684	0.76
8	Al_2O_3	3.0	1052	3882	0.708	0.84
9	SiO_2	0.5	1001	4130	0.620	0.68
10	SiO_2	0.75	1003	4114	0.623	0.70
11	SiO_2	1.0	1009	4100	0.625	0.72
12	SiO_2	1.25	1013	4078	0.628	0.73
13	SiO_2	1.5	1017	4057	0.630	0.75
14	SiO_2	2.0	1024	4027	0.633	0.78
15	SiO_2	3.0	1037	3954	0.643	0.84
16	TiO_2	0.75	1012	4080	0.633	0.66
17	TiO_2	1.0	1019	4033	0.638	0.68
18	TiO_2	1.25	1026	4015	0.643	0.70
19	TiO_2	1.5	1033	3982	0.648	0.73
20	TiO_2	2.0	1045	3937	0.658	0.75
21	TiO_2	3.0	1076	3796	0.680	0.79

been dedicated to the convection of ZnO-EG/DW nanofluids, and significantly much less to the impact of ethylene glycol water mixture base nanofluids on regular convection attributes. A point-by-point examination on thermal conductivity and consistency of ZnO-EG/DW nanofluids against ethylene glycol–water and temperature has been recorded. In addition, the regular convection attributes of ZnO nanofluids were additionally investigated. The regular heat exchange rates for the base fluid water-, EG- or propylene glycol-based nanofluids are compared. In general, water-based fluid + ZnO nanoparticles can provide the benefits of the mixture of two where water + ZnO nanoparticles can upgrade the thermal conductivity and heat exchange properties of the suspension with less sedimentation. In the past, a few investigations were done about thermophysical properties of ZnO-DW-based nanofluids and ZnO dispersion in PEG-water [35].

The key objectives of this research are to prepare the well-dispersed and stable metal oxide-based nanofluids, which include economic and time saving properties for the efficient transportation of heat transfer by using ZnO-DW based nanofluids at 0.1, 0.075, 0.05 and 0.025 mass% concentrations. Single-pot sonochemical synthesis technique was adopted to synthesis ZnO nanoparticles. For longer stability and dispersion of solid nanoparticles in water, a probe sonication technique was employed here. The high probe sonication method helps to increase the dispersion of the particles which increases the stability without using any surfactant. In the present investigation at numerous Reynolds numbers, the localized Nusselt numbers at different points along the test section in the transition and turbulent regions of flow were evaluated for the water base nanofluids at 0.1, 0.075, 0.05 and 0.025 mass% concentrations of ZnO-DW based nanofluids.

Materials and methodology

Zinc acetate-dihydrate ($\text{Zn}(\text{CH}_3\text{COO})_2 \cdot \text{H}_2\text{O}$), and sodium hydroxide (NaOH) were purchased from Sigma-Aldrich M. Sdn Bhd Malaysia Selangor. Ethylene glycol, M. Wt 62.07 g mol was used for ZnO nanoparticle synthesis. All the chemicals used were of analytical grade. Deionized water was used throughout the experiment.

Synthesis of ZnO nanoparticles

The sonochemical synthesis technique was used to prepare the ZnO nanoparticles. In this synthesis, 1M $\text{Zn}(\text{CH}_3\text{COO})_2 \cdot \text{H}_2\text{O}$ precursor was dissolved in mixture of EG@water at 50:50 under constant stirring for 30 min. 2 M (NaOH) base was dissolved in EG@water at 50:50% under constant stirring for 30 min. Finally, the NaOH solution was added dropwise (1 mL min^{-1}) in $\text{Zn}(\text{CH}_3\text{COO})_2 \cdot \text{H}_2\text{O}$ solution under constant sonication [36, 37]. The pulse amplitude was kept at 80% with a 3-s pulse on and 2-s off time span. The power was kept at 750 watts, energy at 36,000 J, and input voltage at 220. During the addition of the NaOH solution into $\text{Zn}(\text{CH}_3\text{COO})_2 \cdot \text{H}_2\text{O}$ solution, white precipitates were formed in the solution. With the passage of time, it is converted into thicker white precipitates. This bulk mixture was sonicated for further 2 h constantly under continuous sonication without using any coolant. The precipitates formed during sonication were washed by DI water 4 times and lastly with ethanol; then it was dehydrated for 2 h at 80 °C temperature. To obtain a discrete shape and morphology of nanoparticles, the sample was needed to be calcined for 3 h at 200 °C temperature (Fig. 1).

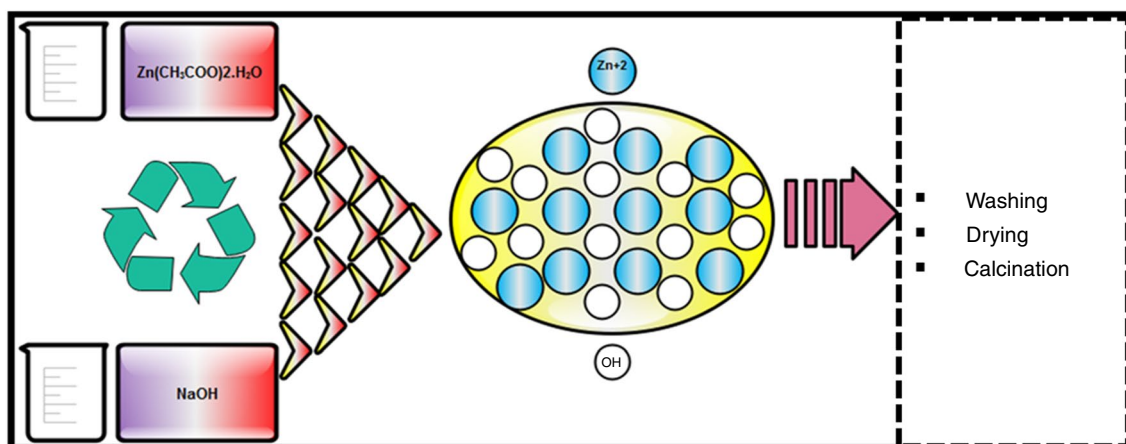


Fig. 1 The synthesis of ZnO nanoparticles by using single-pot sonochemical technique

Preparation of ZnO-DW based nanofluids

A few studies have revealed about the dispersion of zinc oxide nanoparticles in water without adding any surfactant [38]. Suganthi and Rajan [39] reported that ZnO nanoparticles lie around the unbiased pH, so the ZnO nanoparticles dispersed in water are not adequate to oppose agglomeration without a pH change or utilizing a surfactant. However, this does not occur when ZnO nanoparticles are dispersed by utilizing ultra-sonication in polar natural solvents, such as propylene glycol or ethylene glycol as reported by Witharana et al. [40]. Consequently, following the remarks of Suganthi and Rajan [39], nanopowder was added to a pre-determined volume of pure ethylene glycol and sonicated in the ultrasonic shower (probe sonicator having the power of 750w max) for 30 min for dispersion of ZnO nanoparticles. The below-given table describes the ZnO-DW-based nanofluids concentrations (Table 2).

The ZnO-DW-based nanofluids were sonicated by using Prob-sonicator (Input Max 220 V, 20-kHz frequency, amplitude 80, energy (36,000 J) with the pulse rate of 3 s on and 2-s offsetting. Sonication parameters (time and power) optimized for ZnO/water nanofluid having 1 mass% in concentration. All the ZnO/water nanofluid samples of 0.1, 0.075, 0.05 and 0.025 mass% concentrations were sonicated by using (70–90 Watt) power for 30 min. The size of ZnO nanoparticle distribution for given concentrations was measured by Zetasizer (Malvern) based on the dynamically light

Table 2 The ZnO Mass% in base fluid for different concentrations of ZnO-DW based nanofluids for the experiment

S. no	Mass% concentration	Base fluid/L	ZnO nanoparticles/g
1	0.1	7	7
2	0.075	7	5.25
3	0.05	7	3.5
4	0.025	7	1.75

scattering (DLS) process at 298 K and scattering angle of 173° [41]. The stability of different nanoparticles in water was examined by variation of nanoparticles diameter in dispersion and by sonication time. It was observed that the nanofluids at different sonication times could hold different stability and dispersion in the water. When 0.2 mg of ZnO nanoparticles were dispersed in 30 mL water and sonicated for 30 min, 60 min, 90 min and 120 min, different rate of sedimentation was observed in the present investigation (Fig. 2).

Experimental process

Hydrodynamic and convective heat exchange properties of ZnO-DW-based nanofluid were investigated in a square pipe test section of an experimental test rig (Fig. 3) installed in the advanced CFD laboratory in University of Malaya. Prior to run the samples in the test rig, relevant vales, temperature sensors, flow meters, and DP transmitters were checked, calibrated and lined up. The measured pipe surface temperatures at the depth of wall thickness were transferred to the inner surface temperatures of the test pipe by utilizing the Wilson plot [42]. Here, the measured thermophysical properties of ZnO-DW based nanofluids were used for calculating pressure drop (Pa m^{-1}), Nusselt number (Nu), and heat transfer coefficient (h) values (Table 3).

By applying the Newton cooling law, inlet, outlet, and bulk fluid temperatures and surface temperatures, the convective heat transfer coefficient could be calculated, as shown in Eq. (1). Figure 3 shows a complete experimental setup for nanofluid testing with a schematic diagram and flow directions.

Data analysis

Experimental data were used to calculate the heat transfer and pressure drop characteristics, each of the involved fluids. Reynolds (Re) number of distilled water and ZnO-DW-based nanofluids with different concentrations can be deliberated

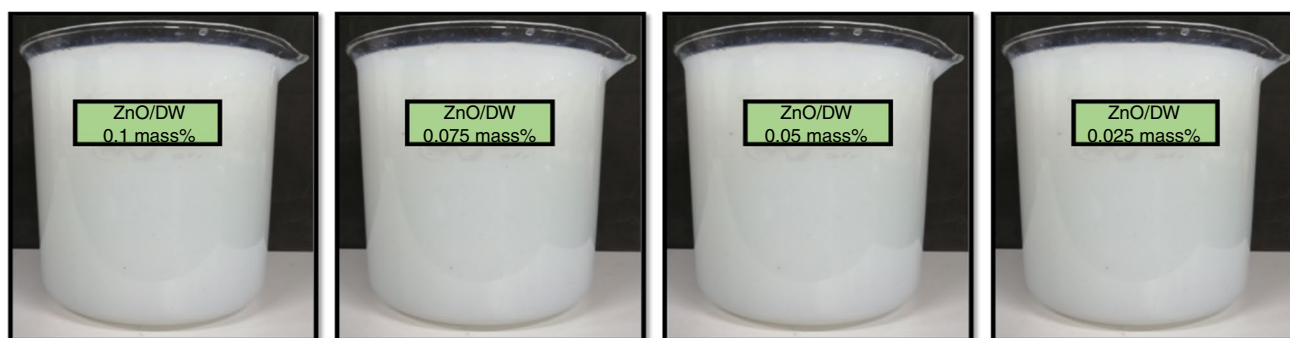


Fig. 2 ZnO-DW based nanofluids (0.1, 0.075, 0.05 and 0.025) mass% concentrations

Fig. 3 Experimental setup for heat transfer measurements of ZnO-DW based nanofluids

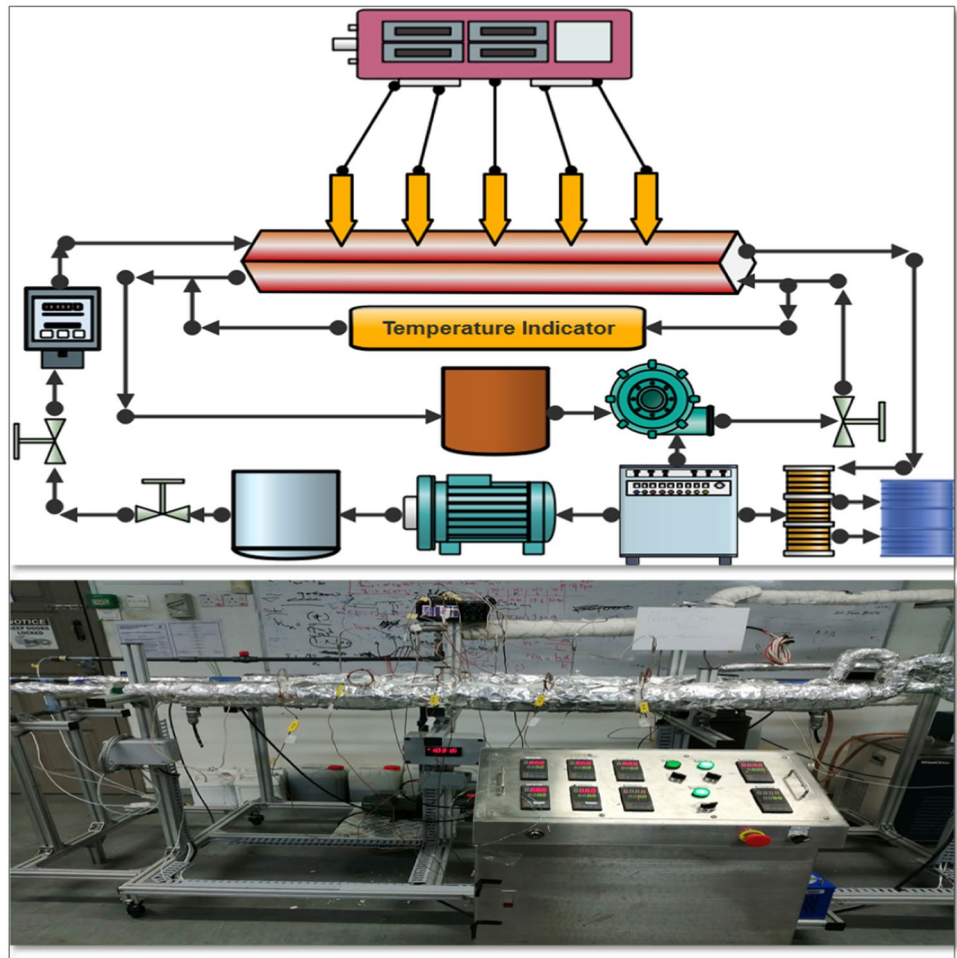


Table 3 Dimensions of the test section

<i>Dimensions of square heat pipe exchangers</i>	
Length of square pipe	1.2 m
Cross section of square pipe	0.01 m
Shape of pipe	Square
No. of thermocouples on the pipe	5
The distance of two thermocouples	0.2 m
Material of square pipe material	Aluminum metal
Height of test section from the ground	1.5 m
<i>Flow conditions of test rig</i>	
Heat flux boundaries conditions	Constant
Flow rates/Reynolds	Variable
External temperature	Room temperature
Test rig input voltage	220 V, AC
Heating power	420 W
Fluid pump frequency	50 Hz
Pump RPM	500
Pump input voltage	220 V

based on experimental setup, hydraulic diameter and mass velocity of the square pipe heat exchanger as given below.

$$h = \left(\frac{q''}{T_w - T_b} \right) \tag{1}$$

where (T_w) , wall temperature; (T_b) , bulk temperature; q , heat flux, (T_b) can be express as $(T_o + T_i/2)$, and here T_o and T_{in} are the outlet and inlet fluid temperatures, respectively.

Heat flux can be calculated by Eq. (2).

$$q'' = \left(\frac{Q}{A} \right) \tag{2}$$

Input power is (Q) , which is the product of the supplied voltage and current $(P = IV)$ for heating the test section. (A) is the internal surface area of the square test section. For the square section, the area can be evaluated by using Eq. (3).

$$A = 4AL \tag{3}$$

For the current experimental setup, maximum input power was kept at (600 W).

Dimension less Nusselt number was calculated by Eq. (4).

$$\text{Nu} = \left(h * \frac{D_h}{K} \right) \quad (4)$$

where Nu, Nusselt numbers; K , thermal conductivity; D_h , hydraulic diameter; h , convective heat transfer coefficient.

For the calculation of local and average Reynolds numbers, Eq. (5) can be used.

$$\text{Re} = \left(\frac{\rho v D}{\mu} \right) \quad (5)$$

Here, Re, Reynolds number; ρ , density; v , velocity; μ , fluid viscosity. For the single-phase nanofluid, the empirical correlation for Nu numbers suggested by Duangthongsuk and Wongwises [43], Gnielinski [44], and Petukhov [45] can be used as presented by Eqs. (8, 6, and 7), respectively.

$$\text{Nu} = \left(\frac{\left(\frac{f}{8} \right) (\text{Re} - 1000) \text{Pr}}{1 + 12.7 \left(\frac{f}{8} \right)^{0.5} (\text{Pr}^{2/3} - 1)} \right) \quad (6)$$

Here, Re, Reynolds number; Pr, Prandtl number; f friction factor.

$$\text{Nu} = \left(\frac{\left(\frac{f}{8} \right) \text{Re} \text{Pr}}{1.07 + 12.7 \left(\frac{f}{8} \right)^{0.5} (\text{Pr}^{2/3} - 1)} \right) \quad (7)$$

If, $3 \times 10^3 < \text{Re} < 5 \times 10^6$ and $0.5 < \text{Pr} < 2000$, then Eq. (6) can be used.

$$\text{Nu} = \left(0.023 \text{Re}^{0.8} \text{Pr}^{0.4} \right) \quad (8)$$

Moreover, Eq. (7) can be used when, $\{\text{Re} > 10^4$ and $0.7 < \text{Pr} < 160\}$.

The friction factor for Eqs. (6 and 7) can be evaluated by the expression of Eq. (9) and the Petukhov friction relationship [45].

$$f = \{(0.79 \ln \text{Re} - 1.64)^{-2}\} \quad (9)$$

However, if $(10^4 < \text{Re} < 10^6)$, the friction factor for ZnO-DW based nanofluids and DI-water could be evaluated from the pressure drop expression of Eq. (10).

$$f = \left(\frac{\Delta P}{\left(\frac{L}{D} \right) \left(\frac{\rho v^2}{2} \right)} \right) \quad (10)$$

where ΔP , change in pressure drop; while v , velocity. The Petukhov empirical co-relation [45] Eq. (9) and the Balsius Eq. (11) for friction factor can be used to evaluate pressure losses.

$$f = (0.3164 \text{Re}^{-0.25}) \quad (11)$$

If, Re numbers are $(3000 < \text{Re} < 10^5)$, then pumping power in the turbulent region can be calculated by using Eq. (12) [46].

$$W = \left\{ 0.158 \left(\frac{4}{\pi} \right)^{1.74} \left(\frac{L m^{2.75} \mu^{0.25}}{\rho^2 D^{4.75}} \right) \right\} \quad (12)$$

where m , mass flow rate in square pipe section.

By putting $(\rho = m/v)$ and $(v = V/A)$ into Eq. (5) and by putting its result into Eq. (12), the resultant pumping power ($W_{\text{nf}}/W_{\text{bf}}$) ratio can be evaluated subsequently at a constant Reynolds number, Eq. (13).

$$\frac{W_{\text{nf}}}{W_{\text{bf}}} = \left(\frac{\rho_{\text{bf}}}{\rho_{\text{nf}}} \right)^2 \left(\frac{\mu_{\text{nf}}}{\mu_{\text{bf}}} \right)^3 \quad (13)$$

where W_{bf} and W_{nf} are the pumping powers for the base fluid and ZnO/water nanofluids, respectively [27].

The thermal conductivity of nanofluids can be calculated by the Hmilton and Crosser [47] equation.

$$k_{\text{nf}} = \frac{k_p + (z-1)k_{\text{bf}} - \phi(z-1)(k_{\text{bf}} - k_p)}{k_p + (z-1)k_{\text{bf}} - \phi(k_{\text{bf}} - k_p)} k_{\text{bf}} \quad (14)$$

Uncertainties in experimental setup

In the current experimentations on ZnO-DW-based nanofluids for heat transfer measurements, the velocity, temperatures, flow rates, pressure drop, Reynolds, Nusselt values, and heat transfer were examined with appropriate tools. During the experimental measurements of these parameters, the uncertainties that happened are reported in Table 4. Seeing the related errors in the separate factors denoted by (x_n) , error estimations of dependent parameters were completed by using the below equation [48]. The net uncertainties were found for proposed experimental results which are given in Table 4. The repeatability approach shows that all parameters of given experimental results are within the uncertainty confines.

$$W = \frac{\left[(x_1)^2 + (x_2)^2 + \dots + (x_n)^2 \right]}{2} \quad (15)$$

Table 4 Uncertainties found during the experiment of the different experimental parameters

S. no	Involved parameters	Symbols	Uncertainty values in%
1	NF inlet temperature	T_{in}	± 0.14
2	NF outlet temperature	T_{out}	± 0.14
3	Ambient temperature	T_e	± 0.14
4	NF mass flow rate	v	± 1.9
5	Pipe diameter	D_h	± 2.0
6	NF differential pressure	h_h	± 2.2
7	NF thermal conductivity	k_{nf}	± 4.4
8	NF viscosity measurement	μ_{nf}	± 3.6
9	NF specific heat measurement	$C_{p,nf}$	± 4.2
10	Voltage	V	± 0.15
11	Current	I	± 0.15
12	Heat flux	Q	± 0.15
13	Power	P	± 0.15
15	Reynolds numbers	Re	± 4.2
16	Convective heat transfer	h	± 3.3
17	Nusselt numbers	Nu	± 4.3
18	Pumping power	P_p	± 4.3

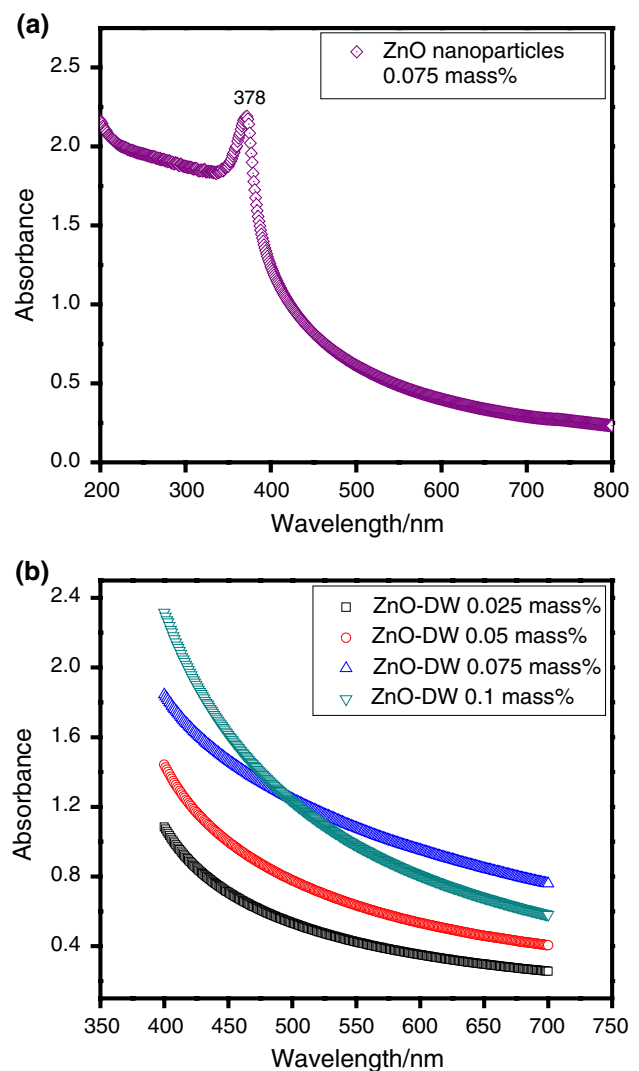
Results and discussion

Characterization of ZnO/EG-water nanofluid

UV–Vis spectroscopy analysis was done to comprehend the optical properties of the sonochemically synthesized ZnO nanoparticles. The UV–visible spectrum of the synthesized ZnO nanoparticles nanofluid of 0.075 mass% concentration is presented in Fig. 4a. The peak at 370 nm indicates the successive formulation of ZnO particles, which is due to blueshifted to the ZnO in bulk. The absorption value increased its bandgap from 3.37 to 3.6 eV. Such enhancement in the band gap is very useful in the presence of sunlight [49].

In Fig. 4b, absorption conduct of different ZnO nanofluids concentrations (0.1, 0.075, 0.05 and 0.025) mass% at normal temperature is displayed. The ZnO nanoparticles are prepared by adapting the standard Probe sonication procedure. The succeeding peak at 370 nm for all the specified concentrations exposes the optimistic formulation of ZnO nanoparticles by using probe sonication method. Different concentrations deviation in absorption levels was due to mass% for each concentration. Rise in mass% enhances the absorption level.

XRD patterns were recorded within a range of 2θ 10° – 90° . XRD patterns were recorded in order to examine the structural crystallinity and purity of ZnO nanoparticles. Figure 5 depicts the XRD patterns of ZnO nanoparticles. Sharp and well-defined characteristic peaks are appeared at


Fig. 4 a UV–Vis spectroscopy of ZnO nanoparticles. b Absorption studies for ZnO-DW based nanofluids (0.1, 0.075, 0.05 and 0.025 mass%) concentrations

2 theta values of {100}, {002}, {102}, {110}, {200}, {112} and {201}, respectively [50], which can be consigned to different crystalline planes of hexagonal crystalline structures of ZnO particles. The sharpen peaks describe the high crystalline index for the prepared ZnO nanoparticles [51].

In Fig. 6, FTIR spectrum is shown for ZnO nanoparticles. The FTIR spectrum confirms the structural analysis with *S. muticum* and different bands. The ZnO nanoparticles synthesized by Probe sonication were examined with the Jacso FTIR5300 model operational at a high resolution about 4000 – 400 cm^{-1} in the presence of transmittance modes. Average absorption in the region of 1627 – 1423 cm^{-1} rotently implies an aromatic ring. Two weak absorption wavelengths of about 2950 – 2790 cm^{-1} describe the occurrence of aromatic aldehydes. The very weak absorption value at 2076 is due to CEC-stretching vibration. The OH stretching values

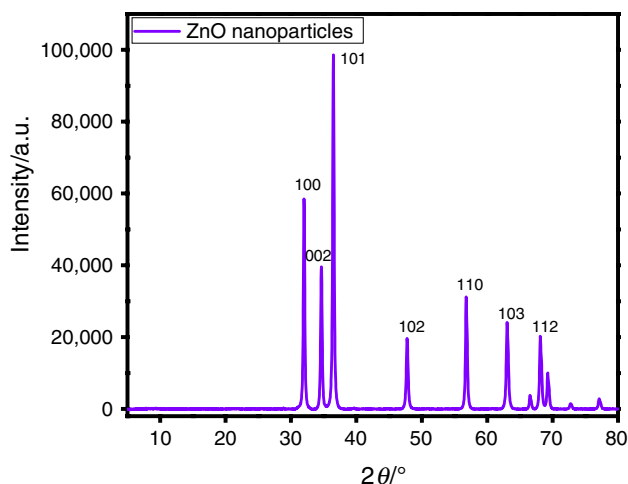


Fig. 5 XRD patterns for ZnO nanoparticles synthesis by probe sonication procedure

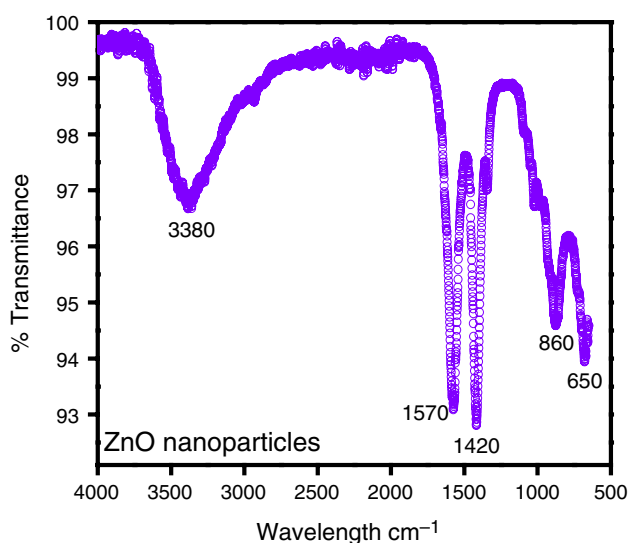


Fig. 6 FTIR analysis of ZnO nanoparticles synthesis by Probe sonication procedure

can be seen at the broad and intensive energy bands at about $3337\text{--}3576\text{ cm}^{-1}$. At the absorption level of $450\text{--}540\text{ cm}^{-1}$, it indicates the presence of ZnO nanoparticles. IR band at 3337 , 1457 , and 2923 cm^{-1} indicates the presence of OH group. In Fig. 6, the FTIR spectra for ZnO nanoparticles (synthesized by co-precipitation method) are shown. Intensive broadband near 3460 cm^{-1} indicates the OH^- vibrations. The band nearer to 2920 cm^{-1} represents asymmetric vibration of alkyl group Csp 3–H.

FESEM image is presented in Fig. 7, which determines the morphological structure, and the elements present in ZnO nanoparticles. Figure 7a shows the spherical and cubic morphology composed of many small particles.

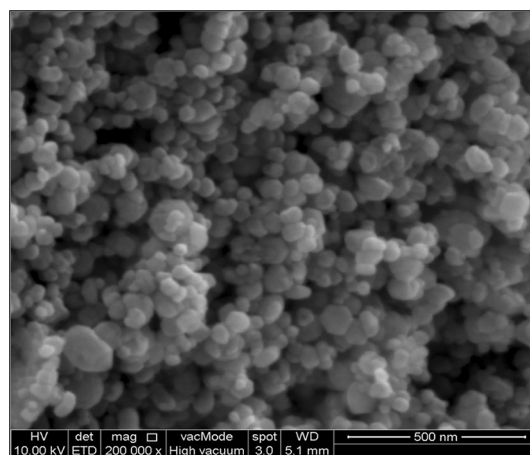


Fig. 7 FESEM analysis of ZnO particles at $\times 100,000$ and 10.00 kv analysis at 100 K magnification, high vacuum and 10.00 kv for ZnO nanoparticles

Figure 7b describes the presence of Zn^{2+} and O^{2-} ions in ZnO nanoparticles. The morphological structure exposed

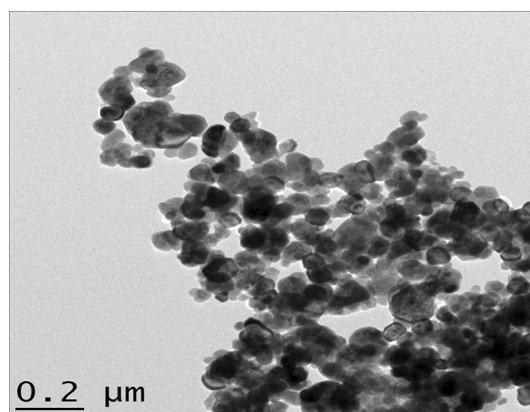


Fig. 8 Transmission electron microscopy (TEM) of zinc oxide nanoparticles synthesized by sonochemical procedure at $\times 300,000$

to the synthesized nanoparticles is in granular shape. The presence of each element can be seen in Fig. 7c. EDX analysis can be examined by Fig. 7b, d; brownish dots represent Zn, and greenish indicates the presence of oxygen ions. FESEM image reveals the uniform and equal distribution of particles, which is due to the physical effect of ultrasonic waves.

The morphological structure of sonochemical synthesized ZnO nanoparticles was assessed by transmission electron microscopy (TEM) and TM G² Tecanai F-30 S TWIN high-resolution transmission electron microscopy (HRTEM) (MIMOS), Kuala Lumpur, Malaysia.

Figure 8 expresses the morphology of (TEM) image of sonochemically produced ZnO nanoparticles. The molecular

size of sonochemical synthesized ZnO nanoparticles perceived from TEM images which are about average 15 nm is generously minor within the display of ultrasound. Additionally TEM of ZnO nanoparticle specifies monodispersed morphology, which is once more attributed to cavitation cases as of ultrasound. The TEM picture obviously designates nanoparticles of ZnO added to one another as an associate to SEM or FESEM images.

Stability and dispersion of zinc oxide nanoparticles in water

Figure 9a predicts the stability of ZnO nanoparticles suspension in water subjected to Probe sonication for different time periods. The probe sonicator (input voltage 220, 20 kHz frequency, amplitude 80, pulse rate is 3 s on/2 s off, energy

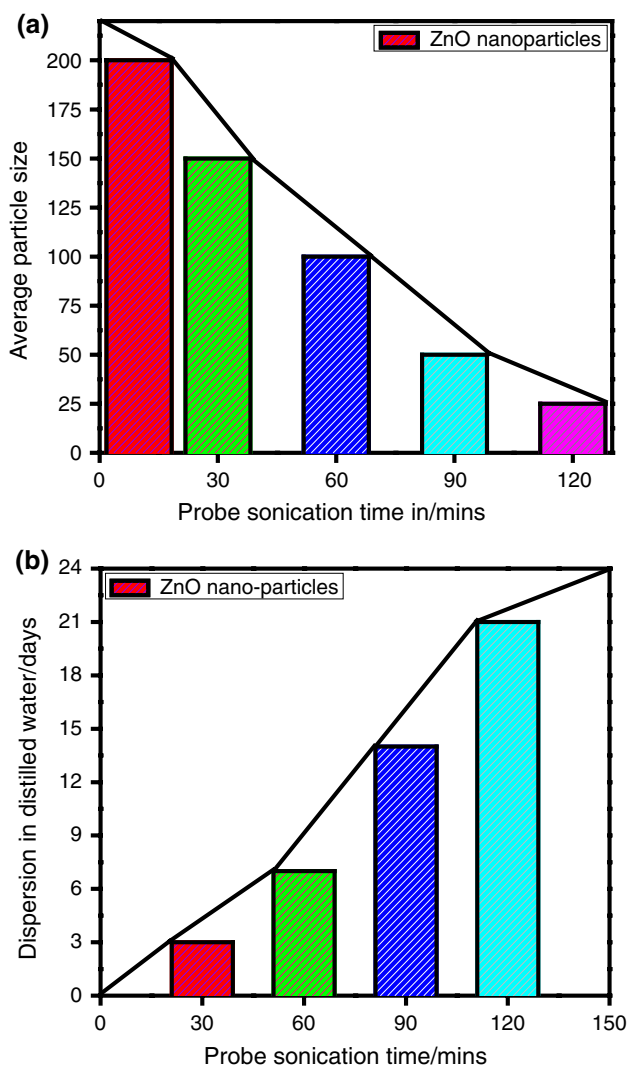


Fig. 9 a ZnO nanoparticle size versus probe sonication time. b Probe sonication time vs dispersion and stability of ZnO nanoparticles

36,000 J, probe-temperature 0 °C, max power 750 W) was used for sonication of ZnO nanoparticles nanofluids for (30, 60, 90 and 120) minutes consecutively. It can be seen from Fig. 8a, b that with the increase in sonication time, the particle size was decreased up to 10–20 nm due to higher shear stress developed by the rotation and simultaneous vibration of the sonicator probe.

For stability test, 0.01 g ZnO nanoparticles were dispersed in 30 mL water and then sonicated for different time span (30, 60, 90 and 120 min) keeping the same machine operating parameters (frequency 20 kHz, input voltage 220, amplitude 80%, energy 36,000 J, pulse rate 3 s on/2 s off). Figure 9b depicts the sonication time against dispersion and stability of ZnO particles in water. A linear trend between sonication time and dispersion/stability shows the dispersion and stability increase with the increase in sonication time.

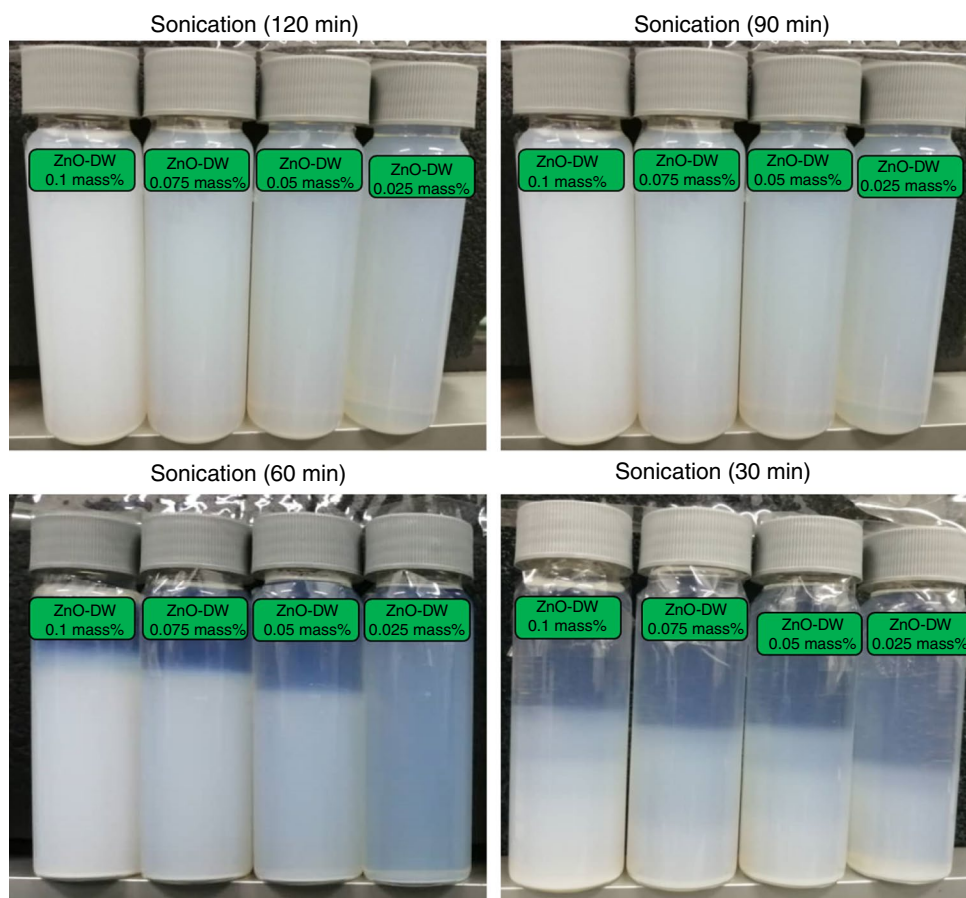
Figure 10 describes the well dispersion of ZnO particles in base fluid (distilled water) where ZnO particles after synthesizing were blended in water according to particular mass% concentrations and highly sonicated to obtain uniform dispersion of nanoparticles. For dispersion investigation, four samples of ZnO particles with varying mass% concentrations (0.1, 0.075, 0.05 and 0.025) were physically examined for dispersion and stability after preparation; each sample has been sonicated according to different time spans (30, 60, 90 and 120 min) by adjusting the probe sonicator specifications like (frequency 20 kHz, IP voltage 220, max amplitude 80, total delivered energy 36,000 J, pulse duration is 3/2 s on-off and temperature 0 °C). The visual observations were conceded on weekly basis, and few images were shot during physical observation as shown in Fig. 10. The images presented all samples which were more sonicated for 120 and 90 min correspondingly showed well dispersion and suspended until 24 days after the day of sonication without mixing any type of surfactant or stabilizing agent. This longer dispersion may be transpired due to the high sonication and maximum presence of nanoparticles in base fluid (distilled water). However, the other two samples show less dispersion and suspension as compared to longer sonicated samples, due to early sedimentation of the nanoparticles inside the base fluid.

Thermophysical and hydrodynamics properties

Figure 11a presents the thermal conductivity at different concentrations (0.1, 0.075, 0.05 and 0.025 mass%) of ZnO-DW-based nanofluid as a function of temperature. The rising trend in Fig. 10 illustrates the growing behavior of thermal conductivity with the increase in temperature and loadings of ZnO nanoparticles in the suspension.

The evaluated thermal conductivities were 0.98 W mK⁻¹ at 45 °C and 0.1 mass%, 0.82 W mK⁻¹ at 45 °C and

Fig. 10 Stability and dispersion of ZnO-DW-based nanofluids with different mass% concentration sonicated for different times (30, 60, 90, 120 min)



0.075 mass%, 0.75 W mK^{-1} at 45 °C and 0.05 mass% and 0.67 W mK^{-1} at 45 °C and 0.025 mass%. Figure 11a represents the linear growing trend of thermal conductivity with the rise of temperature at different concentrations of ZnO nanoparticles in the base fluid. In addition, water holds a fine dispersion of ZnO nanoparticles. The rise of mass% of ZnO nanoparticles enhances the nanofluid thermal conductivity ratio of about 47% at 40 °C for 0.1 mass% loading of ZnO nanoparticles in the base fluid. Further increase in thermal conductivity goes up to 52% higher at 45 °C for 0.1 mass% concentration of ZnO nanoparticles in water. This enhancement occurred due to the increase in Brownian motion of ZnO nanoparticles in the base fluid in the changing temperatures; thus, it augmented the thermal conductivity. Further, with a rise in thermal conductivity with the loadings of ZnO nanoparticles in the base fluid, the existence of more numbers of ZnO nanoparticles in water exhibited a greater effect of heat conduction in the nanofluid. There are many other factors involved to increase the thermal conductivity (a) dispersion of nanoparticles in water, (b) increase in mass% concentration of ZnO nanoparticles, and (c) the internal formation of fluid molecules structured with the ZnO nanoparticles surface, which enhances heat transfer with the ZnO

particles in the base fluid with the formation of homogeneous suspension [52].

Here we also measured specific heat capacity in ($\text{J kg}^{-1} \text{K}^{-1}$) for each concentration of ZnO-DW-based nanofluid in Fig. 11b. The growing trend in the graph described as temperature increased the specific heat for each concentration which will rise linearly. The slope is the same for each concentration-specific heat curves, which refers very well toward findings by Cho and Pak [53, 54]. It can be observed that an increase in mass% of ZnO nanoparticles decreases the specific heat values overall, where the average estimated reduction in specific heat value is 0.42–1.42% compared to water.

Pumping power against each wt. concentration can be seen in Fig. 11c, where growing trends show as mass concentration of ZnO particles increases in water; the motor requires more power to pump the fluid. It can be observed, with low mass concentration low pumping requires for fluid flow. 0.1 mass% ZnO-DW-based nanofluids require maximum pumping power to flow in the test section.

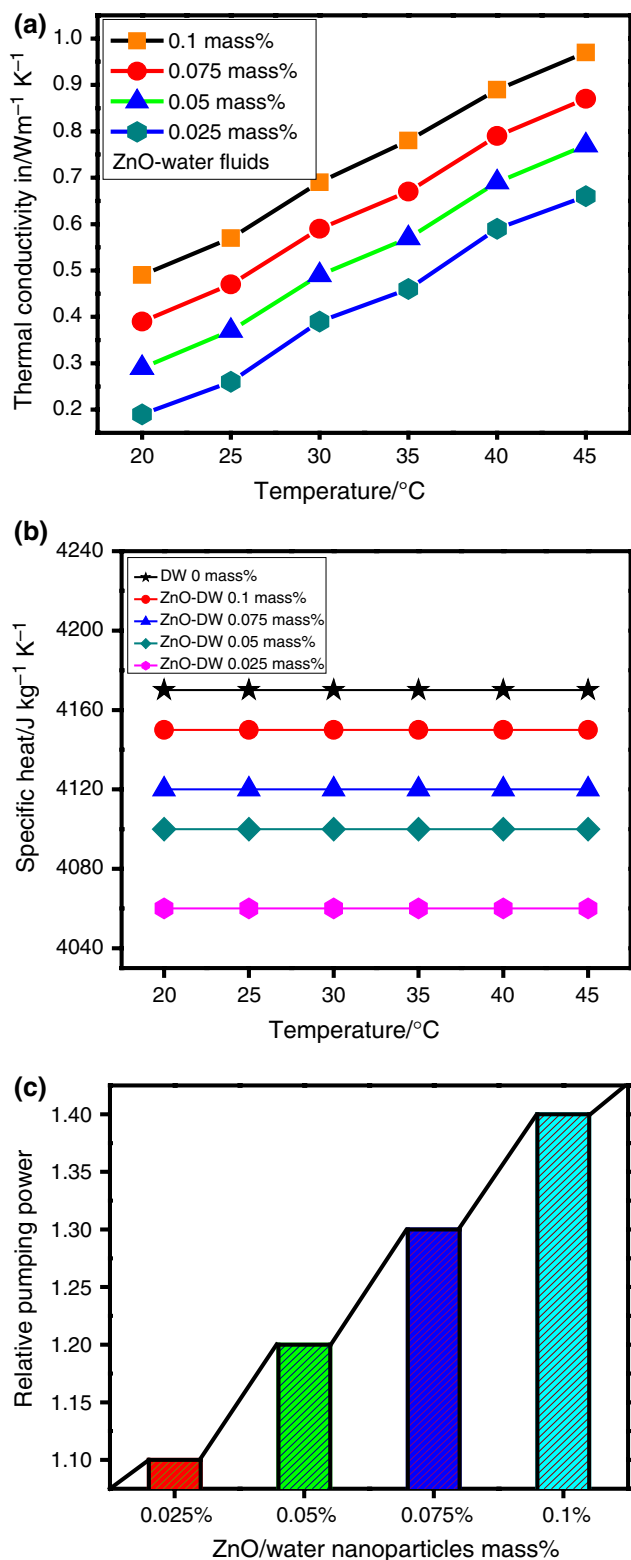


Fig. 11 **a** Thermal conductivity measurements for ZnO-DW based nanofluids (0.1, 0.075, 0.05 and 0.025) mass%. **b** Specific heat capacity variations. **c** Relative pumping power for the flow of nanofluids in the square pipe heat exchanger

Heat transfer properties

The stated literature portrays the addition of numerous types of nanoparticles in the base fluids display enhanced heat transportation and Nusselt numbers [55]. In the present analysis, the effect of mass% of ZnO-DW based nanofluids concentrations (0.025, 0.05, 0.75, and 0.1 mass%) on the average and local heat transfer coefficients at the Reynolds number from 4550 to 20,360 was considered. Figure 12a–d depicts the local behavior of heat transfer for each of the concentrations. For 0.1 mass% concentration of nanofluid, the local heat transfer coefficients obtained from 600 to 1100 W m⁻² K at the Reynolds number ranged from 4550 to 20,367. For 0.075 mass% nanofluid concentration, the local heat transfer coefficients were recorded from 500 to 960 W m⁻² K at the Reynolds number from 4550 to 20,367.

For 0.05 mass% concentration of nanofluid, the heat transfer coefficients were noticed from 500 to 910 W m⁻² K⁻¹ at the Reynolds number ranged from 4550 to 20,367. In Fig. 12d, it can be seen that the local heat transfer coefficients were revealed from 500 to 900 W m⁻² K⁻¹ at the same Reynolds number range specified earlier.

To proceed with the same efforts, average heat transfer was calculated for the nanofluids at each of the specified concentrations for comparison with the base fluid. In Fig. 12e, the growing trends are clearly depicting that the convective heat transfer coefficient is increasing as the mass% nanofluid concentration is increased. For the base fluid, it can be noticed that the heat transfer was low due to the absence of ZnO nanoparticles, as nanoparticles added it increased the average heat transfer coefficient. From given Fig. 12e, it can be easily observed that at 0.1 mass%, the transfer coefficient was greater compared to water data. For the base fluid, it was observed from 500 to 800 W m⁻² K⁻¹, while at 0.1 mass% nanofluid concentration it was much higher and the data varied from 800 to 1100 W m⁻² K⁻¹.

Local and average Nusselt numbers

Figure 13a–d describes the different trends in Local Nusselt numbers with different values of Reynolds numbers (Re) and different concentrations of ZnO-DW based nanofluid like (0.1, 0.075, 0.05, and 0.025 mass%). It was observed experimentally that the local Nusselt numbers increased with the increase of Reynolds number for a straight pipe with the hydraulic diameter similar to the circular pipe diameter. It can be seen in Fig. 13a–d, that at all the specified concentrations of ZnO-DW based nanofluid, the local Nusselt number values are increasing with the increase of Reynolds numbers. For 0.1 mass% nanofluid concentration, the local Nusselt numbers were noticed from 11 to 20 at the Reynolds number ranged from 4550 to 20,367. In the case of 0.075 mass%, an increase in local Nusselt was observed from 9 to 22 for the

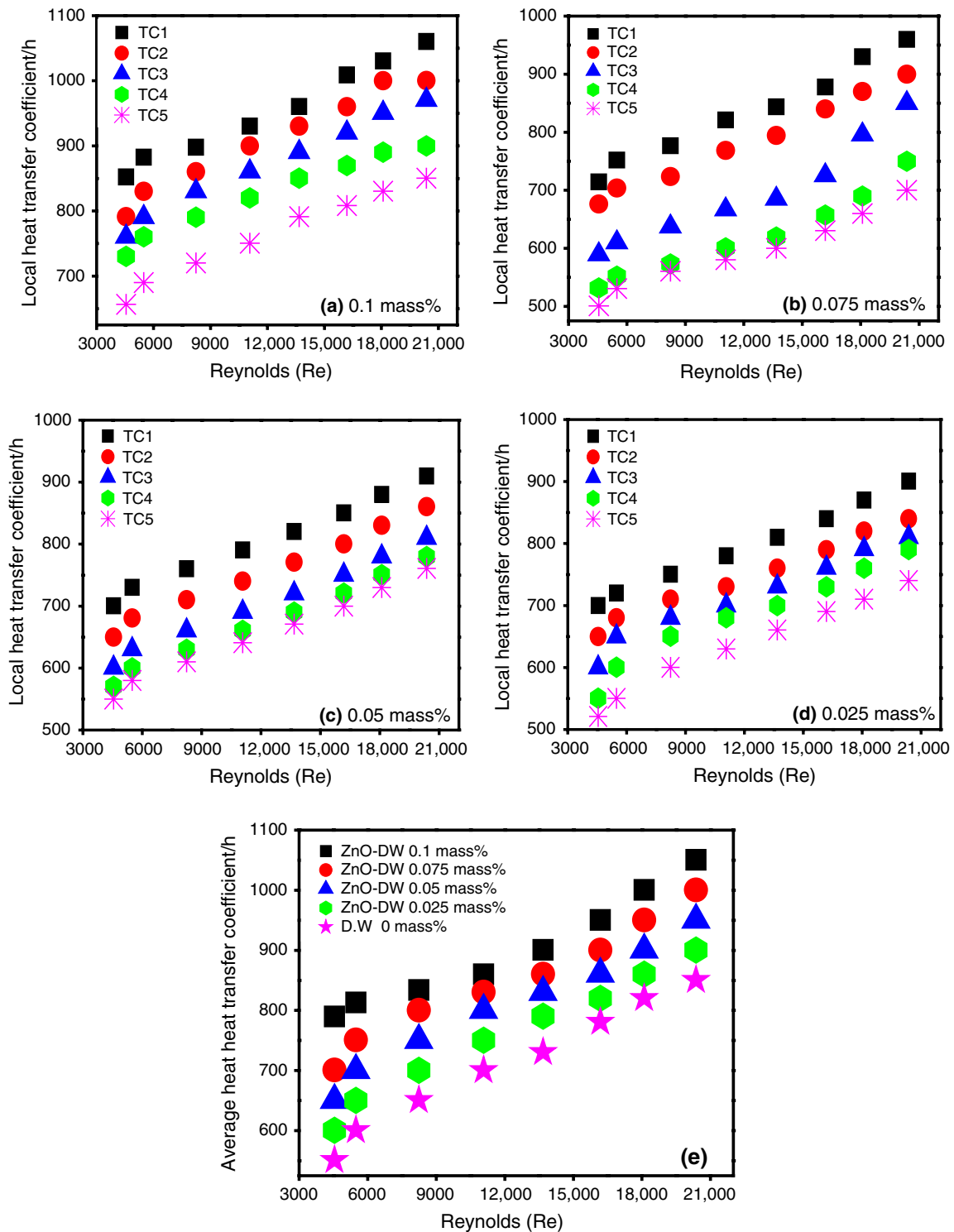


Fig. 12 a Local heat transfer coefficient in $W m^{-2} K^{-1}$ at 0.1 mass% concentration of nanofluid. **b** Local heat transfer coefficient at 0.075 mass% nanofluid concentration. **c** Local heat transfer coef-

cient at 0.05 mass% nanofluid concentration. **d** Local heat transfer coefficient at 0.025 mass% nanofluid concentration and **e** the average heat transfer coefficients at all the specified concentrations

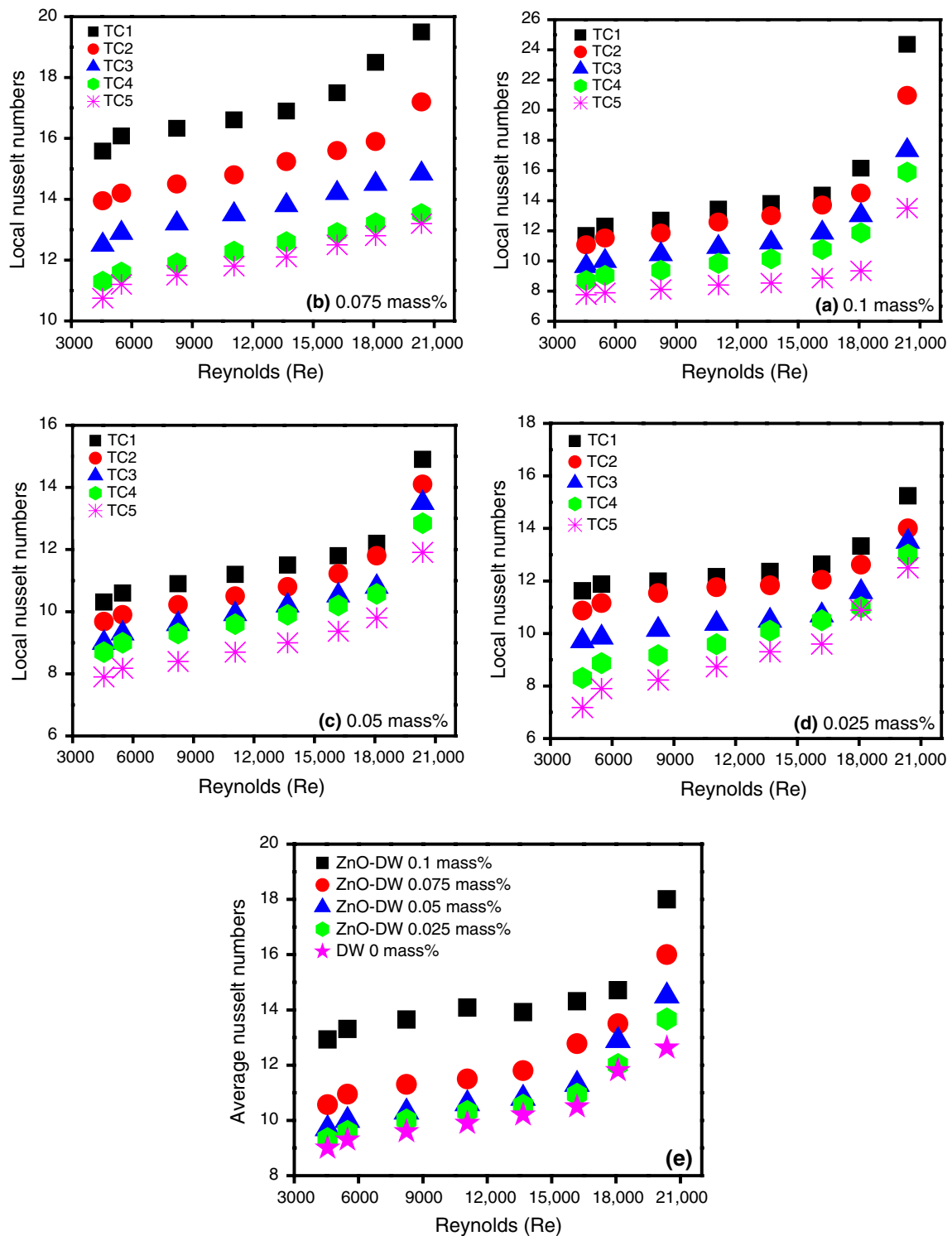


Fig. 13 a Local Nusselt numbers for 0.1 mass% nanofluid concentration. **b** Local Nusselt numbers at 0.075 mass% nanofluid concentration. **c** Local Nusselt numbers at 0.05 mass% nanofluid concentration.

d Local Nusselt numbers at 0.025 mass% nanofluid concentration and **e** the average Nusselt numbers at all the specified concentrations of ZnO-DW-based nanofluids

same Reynolds numbers. For 0.05 mass% concentration of nanofluids, the observed local Nusselt numbers are varied from 8 to 15 against the Reynolds number range from 4550 to 20,367. Finally, for 0.025 mass% nanofluid concentration the local Nusselt number varied from 7 to 15 with the variation of the Reynolds number in the same specified range. This decreasing behavior at lower Reynolds number and concentrations are attributed to the agglomeration effects of ZnO nanoparticles at the lower range of Reynolds number values and lower metal oxide surface areas at the lower concentrations. With higher Reynolds value, the agglomeration effects for ZnO nanoparticles decrease which strengthens the dispersion of nanoparticles in water due to its mixing. Figure 13e depicts the enhancement in average Nusselt numbers for each of the concentrations of ZnO-DW-based nanofluids with the enhancement of the Reynolds numbers (Re) from 4550 to 20,367.

It can be observed that the average Nu for the base fluid varied from 9 to 13 with the enhancement of the Reynolds numbers. After mixing ZnO nanoparticles in the base fluid, the positive enhancement in the Nusselt numbers was observed, which could be attributed to the concentration level. At 0.1 mass% concentration, the maximum enhancement in Nusselt numbers was recorded against the Reynolds numbers varied from 4550 to 20,367. The Nusselt numbers were greater than those recorded for the base fluid alone.

Conclusions

The key conclusion reached based on the presented research work explored the heat transfer coefficient growth for the ZnO-DW based nanofluid flowing in square pipe heat exchanger at constant heat flux boundary condition. The successful synthesis of ZnO nanoparticles was accomplished by sonochemical procedure that accomplished the formation of ZnO particles of sizes 8 to 15 nm, which was validated by XRD, FTIR, FESEM, EDX mapping; TEM and UV–Vis analyses confirmed that the proper syntheses of ZnO particles were done by this procedure. The physical blending of ZnO nanoparticles was utilized to mix them in water; highly probe sonication method is used to increase the dispersion and stability of solid ZnO particles in water without using any surfactant. The designated mass% ranges of ZnO-DW-based nanofluids were 0.1, 0.025, 0.05, and 0.075; the Reynolds number (Re) varied from 4550 to 20,367. The thermal conductivity of ZnO-DW based nanofluids is higher than that of the base fluid and further enhances with the increase in nanofluid mass% concentrations. The substantial improvement in heat transfer and Nusselt numbers could be accomplished with the increase in mass% of ZnO nanoparticles in the base fluid. ZnO-DW based nanofluids could enhance Nusselt number values in comparison to the base

fluids data, where the enhancement could be varied from 50 to 89% in the investigated range of Reynolds number. Thus, improvement in Nusselt numbers, thermal conductivity, and heat transfer properties could support the compatibility of ZnO-DW-based nanofluids as a suitable choice for the heat exchanger liquids in industrial and household applications.

Acknowledgements Authors gratefully acknowledge the UMRG Grant RP045C-17AET, UM Research University Grant GPF050A-2018, Institute of Advanced Studies, Nanotechnology and Catalysis Research Center, and UM Research University Grant GPF017A-2019, Department of Mechanical Engineering and the University of Malaya for the support to conduct this research work.

Compliance with ethical standards

Conflict of interest The author professed that there is no conflict of interest.

References

1. Choi SU, Eastman JA. Enhancing thermal conductivity of fluids with nanoparticles (No. ANL/MSD/CP-84938; CONF-951135-29). Lemont: Argonne National Lab; 1995.
2. Aghahadi MH, Niknejadi M, Toghraie DJ. An experimental study on the rheological behavior of hybrid Tungsten oxide (WO₃)-MWCNTs/engine oil Newtonian nanofluids. *JoMS*. 2019;1197:497–507.
3. Elsaid AM. Experimental study on the heat transfer performance and friction factor characteristics of Co₃O₄ and Al₂O₃ based H₂O/(CH₂OH)₂ nanofluids in a vehicle engine radiator. *Int Commun Heat Mass Transfer*. 2019;108:104263.
4. Xie H, Wang J, Xi T, Liu YJ. Thermal conductivity of suspensions containing nanosized SiC particles. *IJT*. 2002;23(2):571–80.
5. Leong KY, Razali I, Ahmad KK, Ong HC, Ghazali MJ, Rahman MRA. Thermal conductivity of an ethylene glycol/water-based nanofluid with copper-titanium dioxide nanoparticles: an experimental approach. *Int Commun Heat Mass Transfer*. 2018;90:23–8.
6. Pang C, Jung J-Y, Lee JW, Kang YTJ. Thermal conductivity measurement of methanol-based nanofluids with Al₂O₃ and SiO₂ nanoparticles. *IJHMT*. 2012;55(21–22):5597–602.
7. Pourfattah F, Motamedian M, Sheikhzadeh G, Toghraie D, Akbari OA. The numerical investigation of angle of attack of inclined rectangular rib on the turbulent heat transfer of water–Al₂O₃ nanofluid in a tube. *IJMS*. 2017;131:1106–16.
8. Qiu L, Zhu N, Feng Y, Michaelides EE, Żyła G, Jing D, et al. A review of recent advances in thermophysical properties at the nanoscale: from solid state to colloids. *Phys Rep* 2019;843:1–81.
9. Qiu L, Zhu N, Zou H, Feng Y, Zhang X, Tang DJ, et al. Advances in thermal transport properties at nanoscale in China. *IJoH*. 2018;125:413–33.
10. Wen D, Ding Y. Experimental investigation into convective heat transfer of nanofluids at the entrance region under laminar flow conditions. *Int J Heat Mass Transf*. 2004;47(24):5181–8.
11. Sadeghinezhad E, Mehrali M, Tahan Latibari S, Mehrali M, Kazi SN, Oon CS, et al. Experimental investigation of convective heat transfer using graphene nanoplatelet based nanofluids under turbulent flow conditions. *Ind Eng Chem Res*. 2014;53(31):12455–65. <https://doi.org/10.1021/ie501947u>.
12. Elsaid AM. Experimental study on the heat transfer performance and friction factor characteristics of Co₃O₄ and Al₂O₃ based

- H₂O/(CH₂OH)₂ nanofluids in a vehicle engine radiator. *ICHMT*. 2019;108:104263.
13. Abdelrazek AH, Kazi S, Alawi OA, Yusoff N, Oon CS, Ali HM, et al. Heat transfer and pressure drop investigation through pipe with different shapes using different types of nanofluids. *JTAC*. 2020;139:1637–53.
 14. Wen D, Ding YJ. Experimental investigation into convective heat transfer of nanofluids at the entrance region under laminar flow conditions. *IJHMT*. 2004;47(24):5181–8.
 15. Heydari M, Toghraie D, Akbari OA. The effect of semi-attached and offset mid-truncated ribs and water/TiO₂ nanofluid on flow and heat transfer properties in a triangular microchannel. *TSEP*. 2017;2:140–50.
 16. Bai'ri A. Experimental study on enhancement of free convective heat transfer in a tilted hemispherical enclosure by using water–ZnO nanofluid saturated porous materials. *Appl Therm Eng*. 2019;148:992–8.
 17. Sarafraz M, Arya H, Saeedi M, Ahmadi D. Flow boiling heat transfer to MgO-therminol 66 heat transfer fluid: experimental assessment and correlation development. *Appl Therm Eng*. 2018;138:552–62.
 18. Esfe MH, Zabihi F, Rostamian H, Esfandeh S. Experimental investigation and model development of the non-Newtonian behavior of CuO-MWCNT-10w40 hybrid nano-lubricant for lubrication purposes. *J Mol Liq*. 2018;249:677–87.
 19. Shahsavari A, Moradi M, Bahiraei M. Heat transfer and entropy generation optimization for flow of a non-Newtonian hybrid nanofluid containing coated CNT/Fe₃O₄ nanoparticles in a concentric annulus. *Journal of the Taiwan Institute of Chemical Engineers*. 2018;84:28–40.
 20. Shahsavari A, Sardari PT, Toghraie DJ. Free convection heat transfer and entropy generation analysis of water–Fe₃O₄/CNT hybrid nanofluid in a concentric annulus. *Int J Numer Methods Heat & Fluid Flow*. 2019.
 21. Esfe MH, Arani AAA, Madadi MR, Alirezaie A. A study on rheological characteristics of hybrid nano-lubricants containing MWCNT-TiO₂ nanoparticles. *J Mol Liq*. 2018;260:229–36.
 22. Bahiraei M, Godini A, Shahsavari A. Thermal and hydraulic characteristics of a minichannel heat exchanger operated with a non-Newtonian hybrid nanofluid. *Journal of the Taiwan Institute of Chemical Engineers*. 2018;84:149–61.
 23. Huminic G, Huminic A. The influence of hybrid nanofluids on the performances of elliptical tube: recent research and numerical study. *Int J Heat Mass Transf*. 2019;129:132–43.
 24. Afshari A, Akbari M, Toghraie D, Yazdi ME. Experimental investigation of rheological behavior of the hybrid nanofluid of MWCNT-alumina/water (80%)–ethylene-glycol (20%). *JTAC*. 2018;132(2):1001–15.
 25. Aberoumand S, Jafarimoghaddam A. Experimental study on synthesis, stability, thermal conductivity and viscosity of Cu-engine oil nanofluid. *Journal of the Taiwan Institute of Chemical Engineers*. 2017;71:315–22.
 26. Moradi A, Toghraie D, Isfahani AHM, Hosseini AJ. An experimental study on MWCNT-water nanofluids flow and heat transfer in double-pipe heat exchanger using porous media. *JTAC*. 2019;137:1797–807.
 27. Sadri R, Hosseini M, Kazi SN, Bagheri S, Abdelrazek AH, Ahmadi G, et al. A facile, bio-based, novel approach for synthesis of covalently functionalized graphene nanoplatelet nano-coolants toward improved thermo-physical and heat transfer properties. *J Colloid Interface Sci*. 2018;509:140–52.
 28. Yoo D-H, Hong K, Yang H-S. Study of thermal conductivity of nanofluids for the application of heat transfer fluids. *JTA*. 2007;455(1–2):66–9.
 29. Tiwari AK, Ghosh P, Sarkar J. Performance comparison of the plate heat exchanger using different nanofluids. *Exp Thermal Fluid Sci*. 2013;49:141–51.
 30. Ruhani B, Barnoon P, Toghraie DJ. Statistical investigation for developing a new model for rheological behavior of silica-ethylene glycol/water hybrid Newtonian nanofluid using experimental data. *PASMA*. 2019;525:616–27.
 31. Kherbeet AS, Mohammed H, Salman BJ. The effect of nanofluids flow on mixed convection heat transfer over microscale backward-facing step. *IJHMT*. 2012;55(21–22):5870–81.
 32. Hernaiz M, Alonso V, Estellé P, Wu Z, Sundén B, Doretto L, et al. The contact angle of nanofluids as thermophysical property. *J Colloid Interface Sci*. 2019;547:393–406.
 33. Al-Shamani AN, Yazdi MH, Alghoul M, Abed AM, Ruslan MH, Mat S, et al. Nanofluids for improved efficiency in cooling solar collectors—a review. *RSER*. 2014;38:348–67.
 34. Zadeh AD, Toghraie DJ. Experimental investigation for developing a new model for the dynamic viscosity of silver/ethylene glycol nanofluid at different temperatures and solid volume fractions. *JTAC*. 2018;131(2):1449–61.
 35. Suganthi K, Rajan K. ZnO-propylene glycol-water nanofluids with improved properties for potential applications in renewable energy and thermal management. *CSAPEA*. 2016;506:63–73.
 36. Satdeve NS, Ugwekar RP, Bhavase BA. Ultrasound assisted preparation and characterization of Ag supported on ZnO nanoparticles for visible light degradation of methylene blue dye. *J Mol Liq*. 2019;291:111313.
 37. Patil PP, Bohara RA, Meshram JV, Nanaware SG, Pawar SH. Hybrid chitosan-ZnO nanoparticles coated with a sonochemical technique on silk fibroin-PVA composite film: a synergistic antibacterial activity. *IJBM*. 2019;122:1305–12.
 38. Suganthi K, Rajan KJ. Temperature induced changes in ZnO–water nanofluid: zeta potential, size distribution and viscosity profiles. *IJHMT*. 2012;55(25–26):7969–80.
 39. Suganthi K, Rajan KJ. A formulation strategy for preparation of ZnO–propylene glycol–water nanofluids with improved transport properties. *IJHMT*. 2014;71:653–63.
 40. Witharana S, Palabiyik I, Musina Z, Ding YJ. Stability of glycol nanofluids—the theory and experiment. *PT*. 2013;239:72–7.
 41. Fedele L, Colla L, Bobbo S, Barison S, Agresti FJ. Experimental stability analysis of different water-based nanofluids. *NRL*. 2011;6(1):300.
 42. Fernández-Seara J, Uhía FJ, Sieres J, Campo AJ. A general review of the Wilson plot method and its modifications to determine convection coefficients in heat exchange devices. *ATE*. 2007;27(17–18):2745–57.
 43. Duangthongsuk W, Wongwises S. Effect of thermophysical properties models on the predicting of the convective heat transfer coefficient for low concentration nanofluid. *ICHTM*. 2008;35(10):1320–6.
 44. Gnielinski VJ. New equations for heat and mass transfer in the turbulent flow in pipes and channels. *NSrtrA*. 1975;75:8–16.
 45. Petukhov B. Heat transfer and friction in turbulent pipe flow with variable physical properties. *Advances in heat transfer*. Amsterdam: Elsevier; 1970. p. 503–64.
 46. Mansour RB, Galanis N, Nguyen CT. Effect of uncertainties in physical properties on forced convection heat transfer with nanofluids. *ATE*. 2007;27(1):240–9.
 47. Hamilton RL, Crosser OJ. Thermal conductivity of heterogeneous two-component systems. *IECF*. 1962;1(3):187–91.
 48. Holman JP, Gajda WJ. *Experimental methods for engineers*. New York: McGraw-Hill; 2001.
 49. Xu S, Fu L, Pham TSH, Yu A, Han F, Chen L. Preparation of ZnO flower/reduced graphene oxide composite with enhanced photocatalytic performance under sunlight. *CI*. 2015;41(3):4007–13.

50. Patel HE, Sundararajan T, Das SK. An experimental investigation into the thermal conductivity enhancement in oxide and metallic nanofluids. *JNR*. 2010;12(3):1015–31.
51. Patterson A. The Scherrer formula for X-ray particle size determination. *PR*. 1939;56(10):978.
52. Poongavanam GK, Ramalingam V. Characteristics investigation on thermophysical properties of synthesized activated carbon nanoparticles dispersed in solar glycol. *Int J Therm Sci*. 2019;136:15–32.
53. Pak BC, Cho YI. Hydrodynamic and heat transfer study of dispersed fluids with submicron metallic oxide particles. *Experimental Heat Transfer an International Journal*. 1998;11(2):151–70.
54. Amiri A, Sadri R, Shanbedi M, Ahmadi G, Kazi S, Chew B, et al. Synthesis of ethylene glycol-treated graphene nanoplatelets with one-pot, microwave-assisted functionalization for use as a high performance engine coolant. *Energy Convers Manag*. 2015;101:767–77.
55. Goudarzi K, Jamali H. Heat transfer enhancement of Al_2O_3 -EG nanofluid in a car radiator with wire coil inserts. *ATE*. 2017;118:510–7.

Publisher's Note Springer Nature remains neutral with regard to jurisdictional claims in published maps and institutional affiliations.